Available online at www.sciencedirect.com
SCIENCE DIRECT
Polymer 47 (2006) 4798–4810
polymer
www.elsevier.com/locate/polymer

Measuring local viscoelastic properties of complex materials with tapping mode atomic force microscopy

Wensheng Xu [a], Paula M. Wood-Adams [a,*], Christopher G. Robertson [b]

[a] Department of Mechanical and Industrial Engineering, Concordia University, 1455 de Maisonneuve Blvd West, EV004.251, Montreal, Que., Canada H3G 1M8
[b] Bridgestone Americas Center for Research and Technology, 1200 Firestone Parkway, Akron, OH 44317-0001, USA

Received 24 February 2006; received in revised form 12 April 2006; accepted 13 April 2006
Available online 19 May 2006

Abstract

Tapping mode atomic force microscopy is a technique to measure the topography and properties of surfaces involving a micro-cantilever with a tip at one end that is excited into an oscillation near its resonance frequency. The phase lag between the excitation signal and the observed oscillation is sensitive to local mechanical properties under certain experimental conditions. We have found that by using silicon as an internal standard reference surface we can unambiguously relate the phase lag to local viscoelastic properties of a polymeric material. A model describing this relation has been built, validated with experimental data and finally inverted such that it can be used to determine local properties. This allows us to measure high frequency local viscoelastic properties on length scales as small as several nanometers. This technique works well for relatively compliant polymer surfaces with a shear modulus less than about 1 GPa.

Keywords: Thin films; Atomic force microscopy; Viscoelasticity

1. Introduction

Tapping mode atomic force microscopy is a technique to measure the topography and properties of surfaces involving a micro-cantilever with a tip at one end that is excited into an oscillation near its resonance frequency. The cantilever-tip assembly is positioned vertically such that the tip touches the surface at the bottom of its down-stroke and then scanned over the surface. The oscillation of the cantilever is affected by the topography of the surface, the local surface properties and the feed back controller, which maintains the amplitude of the oscillation at a fixed set-point value [1–6]. The vertical movements of the stage needed to maintain constant oscillation amplitude are used to draw the topography image and the phase lag of the oscillation relative to the excitation force is used to draw the phase image [1,2].

The phase image is influenced by three factors: the amplitude ratio set-point, the topography and the material properties. Our interest is the effect of material properties but in order to proceed, it is necessary to understand the other factors as well. These factors all influence the phase image because they influence the interaction force between the tip and the sample surface. We need either to be able to neglect a factor or to describe it mathematically. The influence of topography is small and well investigated [7,8]. If one performs the experiment carefully these effects can be minimized and then neglected as we do here.

The amplitude ratio set-point is the ratio of the engaged amplitude to the free vibration amplitude. As the set-point decreases, the tip–sample interaction force increases. The relation between the phase lag and the set-point is more complicated and has been reported in the literature extensively [1,2,8,9]. Generally speaking, when the set-point decreases from 1 to 0 the phase shift starts off larger than 90° and then decreases to below 90°, and finally increases above 90° again [8,9]. The first reversal is due to the change of the average tip–sample interaction force from attractive to repulsive [1,5,9]. The second reversal is likely due to a change in the vibration mode. In our work, we choose the set-point carefully such that we operate in the region where the average interaction force is repulsive and the simple harmonic oscillator approximation for the vibration is suitable.

The influence of material properties on the phase image has also been studied previously but some questions still exist.

* Corresponding author. Tel.: +1 514 848 2424; fax: +1 514 848 3175.
E-mail address: woodadam@alcor.concordia.ca (P.M. Wood-Adams).

0032-3861/$ - see front matter © 2006 Published by Elsevier Ltd.
doi:10.1016/j.polymer.2006.04.032

Mathematical models have been proposed to describe the probe vibration and the tip–sample interaction [1,7,8,10,11]. The tip–sample interaction is usually considered to be a contact problem between a sphere (the tip) and a plane (the sample) [1,7,8,12,13]. In order to describe these models, we refer to Fig. 1, which illustrates the geometry of the problem.

Garcia et al. [12] and Robert et al. [13] use a model where the tip–sample interaction force consists only of an elastic response and an attractive van der Waals interaction. This model explains the first phase reversal described above when the set-point is near 1. It also describes the influence of the free vibration amplitude on the reversal behavior. Scott et al. [8] and Tamayo et al. [7] have incorporated the viscous resistance to tip penetration with approximate analyses of the flow kinematics. Dubourg et al. [10,11] proposed a viscous force model derived from Stokes equation and then modified it for polymeric liquids by incorporating an approximation of the Rouse model.

We use a similar approach as that of Dubourg et al. [10,11] in that we begin from Stokes equation but we do not follow their approach to account for changes in local relaxation time with indentation depth. Instead, we let the viscoelastic properties (both modulus and viscosity) depend on the contact time as explained in more detail later. In general, as contact time increases (i.e. as the tip penetrate deeper) the viscosity increases and the modulus decreases. By combining the model of viscous resistance to indentation with the elastic response and the van der Waals attractive interaction, we build a comprehensive model of the tip–sample interaction force. We combine this with the simple harmonic oscillation model and a feed back control loop to maintain constant amplitude and then simulate the process of the probe scanning on a surface with silicon and polymer domains of different properties. In this way, we study the effect of viscoelastic properties on the vibration behavior of the tip-cantilever assembly focusing in particular on the phase lag. The simulation results are then compared with experimental results and final a technique for determining local viscoelastic properties from phase images is developed. The absolute phase lag is affected by various phenomena in the experiment that are not included in the model such as the effect of a layer of condensed water on the sample surface. To reduce the impact of these non-idealities we use the phase contrast between the polymer domain and that of the silicon domain to compare model and experiment and to develop our technique for determining local viscoelastic properties. In fact, it is known that the presence of a layer of water will induce a capillary force on the tip, $F_{cap}=4\pi R\gamma\cos(\theta)$, where R is the tip radius, γ is the surface tension of water and θ is its contact angle with the sample [2]. The only parameter here that is dependant on the sample material is the contact angle. By neglecting this force and using silicon as an internal reference for our technique we are in effect neglecting the difference between the contact angle of water on the material of interest and that of water on silicon. We consider that this is an acceptable assumption.

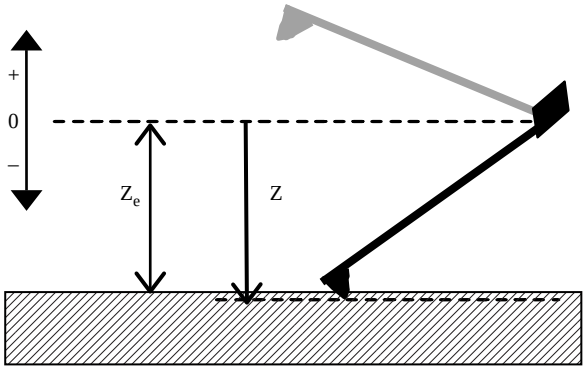

Fig. 1. Geometry of oscillating cantilever-tip assembly. The coordinate Z indicates the vertical distance between the tip and the equilibrium position ($Z=0$). Z_e is the distance between the end of the cantilever and the sample surface and is a positive number. Not shown on this schematic is a_0, the atomic radius of the sample. The indentation depth when the tip is in contact with the surface is: $\delta=a_0-Z-Z_e$.

2. Model for TM-AFM on viscoelastic surfaces

In the harmonic oscillator approximation, the probe vibration and the tip–sample interaction is described by the following equation

$$m\frac{d^2z}{dt^2}+\frac{m\omega_0}{Q}\frac{dz}{dt}+kz=F_0\sin\omega t+F_{ts}(t,z) \quad (1)$$

where z is the tip position at time, t. The parameters m, ω_0, Q, k are the effective mass of tip-cantilever assembly, its angular resonance frequency, quality factor and effective spring constant, respectively. The activation force is $F_0\sin\omega t$ and the tip–sample interaction force is F_{ts}. When the tip is not in contact with the surface, the tip–sample interaction force consists solely of the attractive van der Waals force. For modeling this force, we can treat the tip and sample surface as a sphere–flat plane geometry. Then the tip–sample interaction force under non-contact conditions is

$$F_{ts}=F_{van}=-\frac{HR}{6(z_e+z)^2} \quad (z_e+z>a_0) \quad (2)$$

where H is the Hamaker constant; z_e and z are the tip equilibrium position and its instantaneous position, respectively, and a_0 is the average van der Waals radius of the sample and tip atoms.

When the tip is in contact with the sample surface, the tip–sample interaction force consists of the van der Waals force, the elastic repulsive force, and the viscous repulsive force. The van der Waals force and the elastic repulsive force can be described by the Derjaguin–Muller–Toporov (DMT) model (first two terms of Eq. (4)). According to Stokes equation, when the tip radius R is equal to or greater than the indentation depth, δ, the force caused by the viscous resistance is:

$$F_{vis}=3\pi\eta\delta\frac{dz}{dt} \quad \text{where } \delta=a_0-z-z_e \quad (3)$$

where η is the viscosit; which changes with indentation time as explained later. Finally, the total tip–sample interaction force

during contact is

$$F_{ts} = -\frac{HR}{6(a_0)^2} + \frac{4}{3}E^*\sqrt{R}\delta^{3/2} + 3\pi\eta\delta\frac{dz}{dt} \quad (z_e + z \le a_0)$$

$$\frac{1}{E^*} = \frac{(1-\nu_t^2)}{E_t} - \frac{(1-\nu_s^2)}{E_s} \tag{4}$$

where E^*, E_t, E_s, are the effective tip–sample modulus, the tip modulus and the sample modulus, respectively, and ν_s and ν_t are the Poisson ratios of the sample and the tip.

The time, t_c, when the tip is in contact with the sample surface is only a small fraction of the probe oscillation period. We use the inverse of the contact time as an estimate of the shear rate and then assume that the Cox Merz rule is applicable (Eq. (5)) to estimate the viscosity of the sample under these conditions. The viscosity is then related to the loss and storage modulus as shown in Eq. (6).

$$\eta(\dot{\gamma}) = |\eta^*(\omega)| \quad \text{where } \frac{1}{t_c} = \dot{\gamma} = \omega \tag{5}$$

$$\eta = \sqrt{(G't_c)^2 + (G''t_c)^2} \tag{6}$$

Note that the Young's modulus for a viscoelastic surface is estimated from the storage modulus as shown below.

$$E \cong 2(1+\nu)G' \tag{7}$$

3. Experimental methodology

3.1. Materials and viscoelastic characterization

We have performed experimental studies with the polymers shown in Tables 1 and 2, which include a monodisperse polybutadiene (PB), a polystyrene (PS), and a butadiene–styrene–butadiene block copolymer PB–PS–PB. The polybutadiene and the polystyrene were chosen to validate our model since they represent a very soft (PB) and a very stiff (PS) viscoelastic material at room temperature while the block copolymer was included to compare the behavior of microphase separated domains with that of the pure polymers.

The PB was synthesized by anionic polymerization of 1,3-butadiene in hexane using *s*-butyl lithium as an initiator. The reaction was carried out in a 19 L lab-scale batch reactor at 55–60 °C for 1.5 h. The living polymer—lithium cement was discharged from the reactor into isopropanol to terminate polymerization and serve as a coagulation step. A small amount (1000 ppm relative to polymer weight) of BHT antioxidant was added to the isopropanol prior to termination/coagulation to help protect the subsequently isolated and dried polymer from thermal-oxidative attack.

The microstructure of the polybutadiene was analyzed using ^{1}H and ^{13}C NMR (Varian Mercury 300 NMR) with deuterated chloroform as solvent. The glass transition temperature, $T_g = -93.1$ °C, was measured by differential scanning calorimetry (TA Instruments DSC 2910) at a heating rate of 5 °C/min after cooling at the same rate. Gel permeation chromatography (GPC) was performed in THF using a Waters Model 150 °C with a refractive index detector. GPC measurements were conducted relative to polystyrene standards, and the results were then converted to absolute molecular weight information by applying the universal calibration approach using data concerning the molecular weight dependence of intrinsic viscosity. The molecular weight and microstructure characteristics, which describe the polybutadiene are summarized in Table 1.

Oscillatory shear measurements were conducted to investigate the linear viscoelastic behavior of the polybutadiene. Testing was accomplished in a nitrogen-purged environment using a Rheometrics ARES instrument fitted with two force rebalance transducers with maximum torques of 200 and 2000 g cm. All strains were within the linear viscoelastic region as revealed by strain sweeps. Thermal stability of the polymer at the highest temperature of 75 °C was verified by a rheological time sweep at a constant frequency of 0.03 rad/s. For the formation of the master curves in Fig. 2, the values of the horizontal shift factor, a_T, were determined by superposition of the phase angle data with the results of the vertical shift factor, b_T, subsequently evaluated from the minor vertical adjustments necessary to superimpose the modulus functions.

The polystyrene was obtained from The Dow Chemical Company and is one of their commercial products (Styron 685D). Its molecular characteristics are shown in Table 1. The viscoelastic characterization of this material was carried out at room temperature and below using solid sample torsion clamps on an Anton Paar MCR 500 rotational rheometer. As expected for this glassy polymer, the storage (1000 MPa) and loss (20 MPa) moduli are independent of frequency and only slightly dependent on temperature (through the modulus temperature dependence).

The butadiene–styrene–butadiene block copolymer was purchased from Polymer Source, Montreal, Canada. Molecular structure data and synthesis procedure were provided by the supplier. The block copolymer was prepared by living anionic polymerization with sequence addition of butadiene (predominantly 1,4 addition) followed by styrene and then butadiene again. The molecular weight and polydispersity index of the

Table 1
Characteristics of the polymers

Polymer	Molecular weight		Microstructure		
	M_w (kg/mol)	M_w/M_n			
PB	78.2	1.04	8.8% Vinyl [1,2]	53.5% trans [1,4]	37.7% cis [1,4]
PB–PS–PB	65–25–94	1.07	1,4 Addition		
PS	310.7	2.2			

Table 2
Simulation parameters

Tip and cantilever					
E_t	R	Q	ω_0	K	ν_t
129 GPa	10 nm	400	$680\pi\times 10^3$ rad/s	40 N/m	0.28
Silicon surface					
E_s		a_0		ν_s	
70 GPa		0.234 nm		0.28	
Polybutadiene surface					
$G'(5\times10^7$ rad/s)		$G''(5\times10^7$ rad/s)		ν_s	
4.27 MPa		7.94 MPa		0.5	
Polystyrene surface					
G'		G''		ν_s	
1000 MPa		20 MPa		0.3	

final polymer, the first polybutadiene sequence and the di-block intermediate were determined by size exclusion chromatography (SEC) using a Varian liquid chromatograph equipped with a UV and refractive index detector.

3.2. Atomic force microscopy

Experiments were carried out with a MultiMode SPM of Veeco Metrology Group operating in tapping mode at room temperature under atmospheric conditions. The probe was silicon backside Al-coated from MikroMasch USA. For the AFM studies, we use a flat silicon surface as our internal standard surface to compare with the response of the polymer surface. The silicon substrate was purchased from MEMC Electronic Materials Inc. The polymers were cast from 0.05% solutions in dichloromethane onto the silicon surface and dried for several minutes before imaging. The resulting polymer films were between 20 and 500 nm thick and only covered a potion (normally a circle of 1 to 5 μm in diameter) of the silicon surface. This allowed us to access silicon regions and polymer regions of constant or varying thickness in one TM-AFM image. Film thickness is evaluated relative to the silicon domains using TM-AFM topography images produced with a set-point of 0.9.

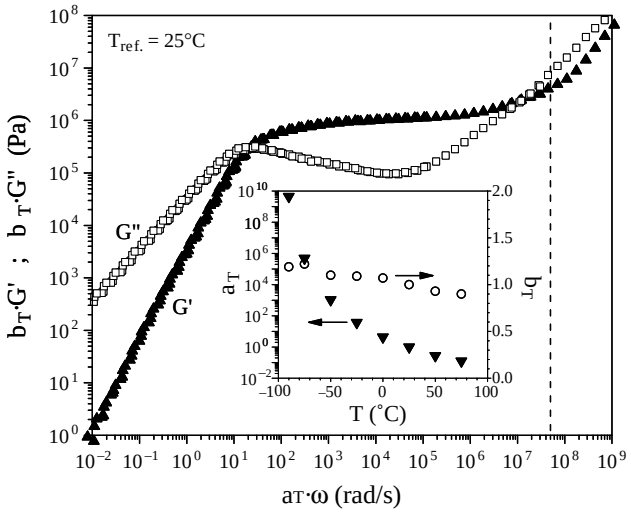

Fig. 2. Master curve at 25 °C for polybutadiene.

4. Simulation of scanning process

We have combined the model presented above with a feed back controller to maintain a constant oscillation amplitude and then simulated the process of the tip scanning over a surface that consists of domains of silicon, polybutadiene and polystyrene using Matlab Simulink. Table 2 shows the parameters for the probe and the surfaces. The parameters of the probe were provided by the manufacturer (MicroMasch USA) and those of the surface were taken from the literature assuming that we have a layer of silica on the surface of the silicon [13]. The mechanical properties of PB (Fig. 2) and PS were obtained from dynamic linear viscoelastic measurements in shear assuming $\omega = 1/t_c$ for the PB. The PS properties are independent of frequency: $G' = 1000$ MPa and $G'' = 20$ MPa. The PS properties were measured over the frequency range of 1–500 rad/s at several temperatures between −80 and 25 °C. At all temperatures the moduli were independent of frequency and except for the modulus shift, independent of temperature. The values reported here were measured at 25 °C between 1 and 500 rad/s, the use of these values at much higher frequencies is justified by the low temperature results. The tip–sample contact time scale is on the order of 10^{-6} s, exact values are determined numerically by iteration.

The scanning process that we simulate is sketched in Fig. 3. For the first 4 ms the tip is vibrating freely, i.e. without contacting a surface, with an amplitude of 90 nm. At 4 ms the set-point is set to 0.6 and the tip is brought into contact with the silicon surface. It vibrates in contact with the silicon surface until 10 ms and then the surface is switched to polybutadiene. At 16 ms the surface changes to polystyrene and the simulation finishes at 22 ms. The set-point is maintained at 0.6 during the entire simulation except for the first 4 ms. The results are shown in Fig. 4.

The tip–sample separation is shown in Fig. 4(a). This curve represents the vertical movements made by the stage in response to the controller. During the free vibration period (0–4 ms) the tip sample separation is constant at 92 nm and the oscillation amplitude (Fig. 4(b)) is 90 nm. It is clear that the tip does not touch the surface under these conditions. As expected for forced vibration near resonance, the phase shift during this period is 90° (Fig. 4(c)).

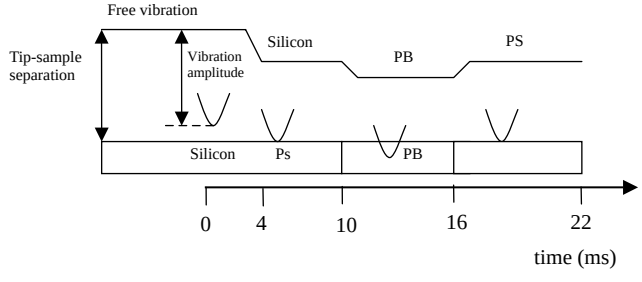

Fig. 3. Scanning process for simulation.

At 4 ms when the set-point is set to 0.6, the tip–sample separation is reduced until the oscillation amplitude is damped to 54 nm because of the interaction of the tip with the silicon surface. The steady state value for the phase shift during this period is 36.5° and the tip–sample separation is 53.5 nm. This indicates that the tip indents 0.5 nm into the silicon surface.

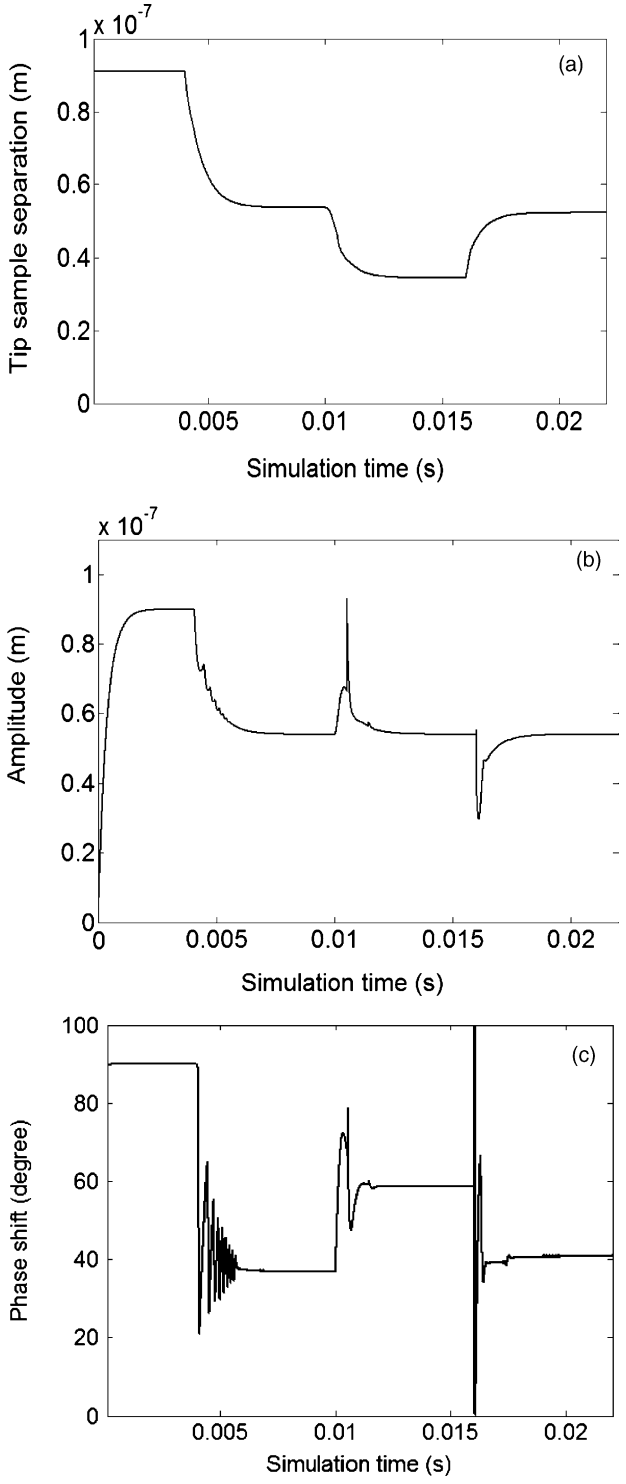

Fig. 4. Simulation results of tip in contact with the surfaces of different materials properties. (a) Tip–sample separation; (b) amplitude curve and (c) phase lag.

During the period 10 ms $< t <$ 16 ms, the tip is vibrating in contact with the polybutadiene surface. Because the polybutadiene is very soft, the tip indents about 19 nm into the surface as indicated by the tip–sample separation of 35 nm. The phase shift during this period is 58.2°. For $t \geqq 16$ ms the tip is in contact with the polystyrene surface. The tip–sample separation is 52.8 nm indicating an indentation depth of 1.2 nm. The phase shift during this period is 41.5°.

In order to compare the simulation results with experimental results, we define the phase contrast with respect to silicon, ϕ, which is simply the difference between the phase shift of the surface of interest and that of silicon. From our simulations, we predict that the phase contrast of PB should be 19° and that of PS should be 4°.

Another useful aspect of our simulations is that we can look at the relative importance of the different tip–sample interaction forces for different materials. Fig. 5 shows the forces acting on the tip over one oscillation cycle for (a) the silicon surface, (b) the PB surface and (c) the PS surface. On the silicon surface, the dominant tip–sample interaction force is the elastic force and on the PB surface it is the viscous force. For the PS surface, both the elastic and the viscous forces are large. The results in Fig. 5 also show that the tip–sample contact time is the longest for the PB surface and the shortest for the silicon surface.

5. Tapping mode AFM experimental studies

In the first series of experiments, we studied the effect of set-point on the phase contrast for PB by disabling the y-axis motion and scanning back and forth over the same line in the x-direction. The probe vibration amplitude was 90 nm in free vibration. Initially, we scanned the same line 256 times at a set-point of 0.6 and produced the topography and phase images shown in Fig. 6. The PB film shows as a bright region in both images because it is higher both in height and phase than the silicon regions. Since, the PB film appears as a bright band of unchanging width, height and phase we can conclude that scanning over the same line multiple times under these conditions does not appreciably disturb the PB film.

Fig. 7(b) shows the phase section of the image in Fig. 6(b), indicating that the phase contrast between PB and silicon is 20° at a set-point of 0.6. Fig. 7(a) shows the topography section of the image in Fig. 6(a) and an image obtained at set-point 0.9 in exactly the same manner. At set-point = 0.9, the net force between the tip and sample is attractive, and we suppose that the indentation depth on the PB is small. Therefore, we assume that the true shape of the PB film is observed in the topography image at set-point = 0.9, while at a set-point of 0.6 the measured heights are the actual heights less the indentation depth. Therefore, for set-points less than 0.9 we calculate the indentation depths from the following:

$$\delta_{\mathrm{Sp}} = h_{0.9} - h_{\mathrm{Sp}} \tag{8}$$

where the subscripts refer to the set-point values and h indicates height. It is important to note that we are likely

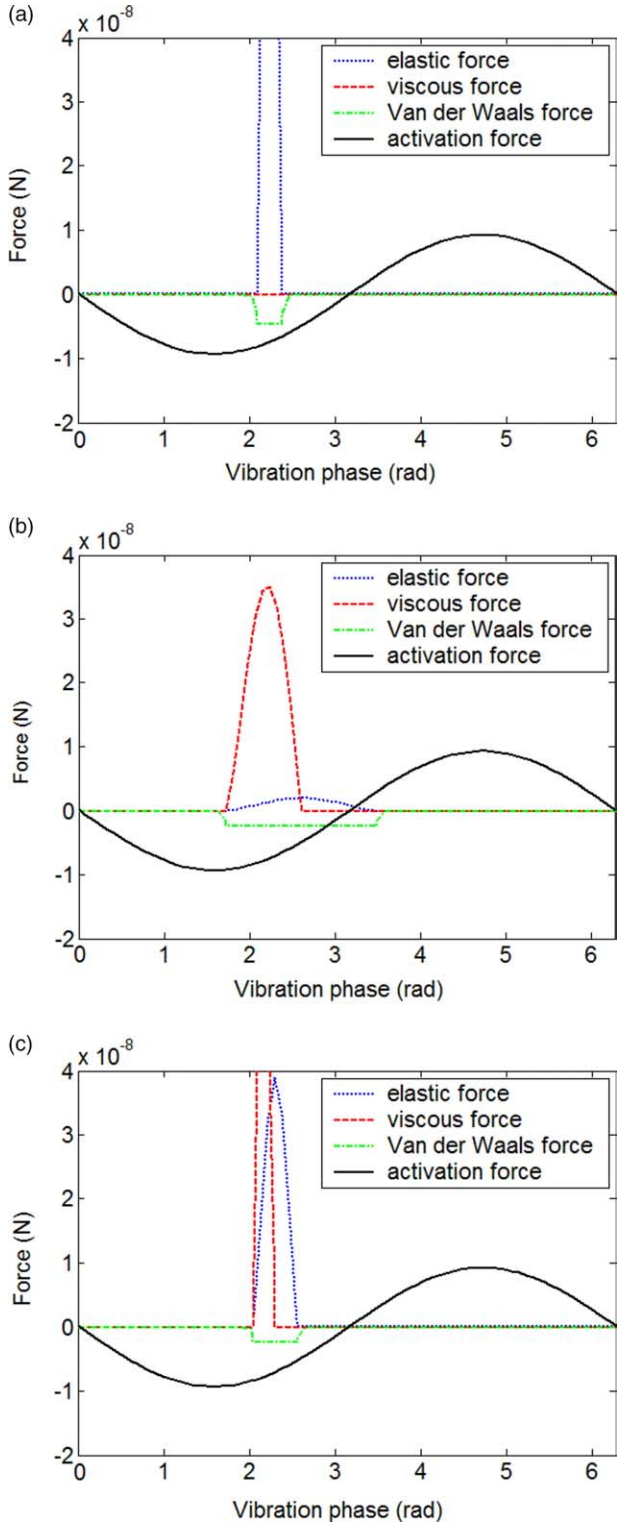

Fig. 5. The force acting on the tip in one vibration cycle. (a) Silicon surface. (b) PB surface. (c) PS surface.

introducing a small offset (on the order of a few nanometers) into all of the indentation depth values by assuming that there is no indentation at a set-point = 0.9. Using this approach, we have acquired the indentation depth and phase contrast for different set-point for PB and compared the results with simulations in Fig. 8.

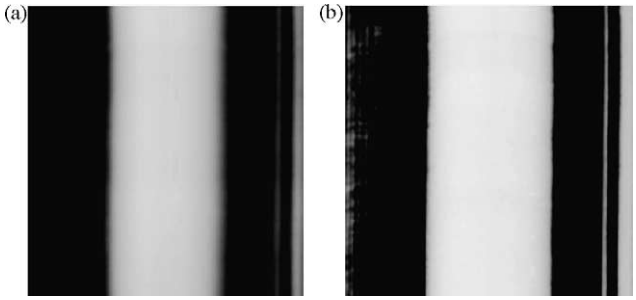

Fig. 6. (a) Topography and (b) phase image of the same horizontal line scanned 256 times. Polybutadiene (light areas) on silicon. Set-point 0.6, free vibration amplitude 90 nm. Grayscale is 0–150 nm for topography image and 0–50° for phase image.

In the experimental curve, when the set-point is 0.95, the phase contrast is negative because of the attractive surface forces. When the set-point is 0.9, the phase is positive but small, indicating that the average tip–sample interaction force is repulsive and very small. When the set-point decreases below 0.5, the phase contrast reverses again, likely because when the tapping force increases the cantilever deforms significantly and the adhesive forces tend to trap the tip on the surface, both of which result in a more complicated vibration of the tip than our model considers. The results in Fig. 8 show that the experimental data and the simulation agree well when the set-point is in the range of 0.5–0.7. This is because the dominant force is repulsive and the probe vibration is simple, both conditions, which are properly described by our model.

We performed a similar study with PS and the results are compared with the simulations in Fig. 9. In this case, we were able to get an accurate measurement of the indentation depth, $\delta = 1$ nm, at a set-point of 0.9. At lower set-points the indentation depth increases only slightly. Note that since we measure an indentation depth of 1 nm on PS at a set-point of 0.9 it is likely that the true indentation in PB at the same set-point is larger than 1 nm. As for PB, the simulation agrees very well with the experimental data for PS over the set-point range of 0.5–0.7.

In the next experiment, we prepared a polybutadiene film of varying thickness to evaluate the effect of this variable. The images of this film are shown in Fig. 10. From the topography image (Fig. 10(a)), we can see that the PB film is thicker at the bottom of the image and thinner at the top. Next, we take a section along the dotted line shown in Fig. 10 to obtain the data shown in Fig. 11. The film thickness varies from a maximum of about 170 nm to a minimum of about 18 nm. In Fig. 11(b) we see that when the film is less than 63 nm thick, the phase contrast becomes dependant on the thickness. This critical thickness corresponds to six times the radius of gyration of this polybutadiene or in other words the film is approximately three molecules thick. All other experiments, including those presented earlier in this section were performed on films thick enough such that the phase contrast was independent of the thickness. Note that the measurements of film thickness

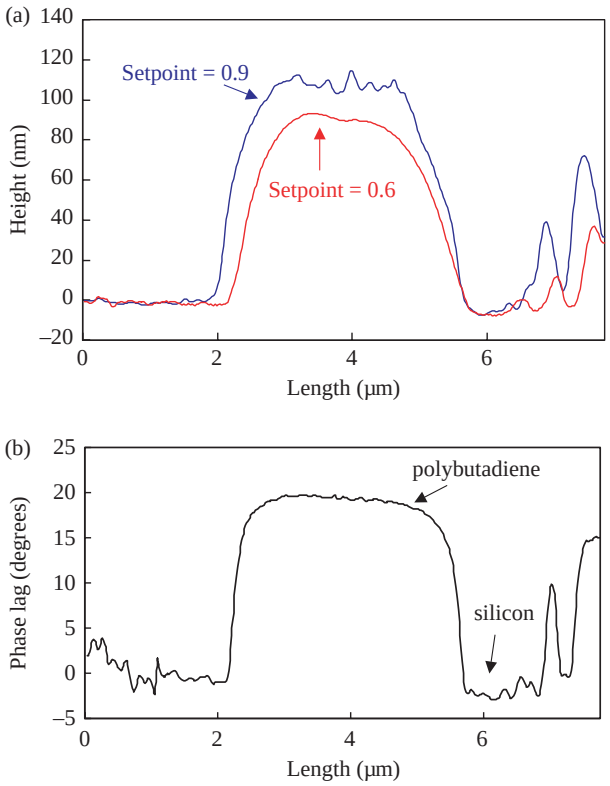

Fig. 7. Sections of the (a) topography and (b) phase images in Fig. 6 and another topography image taken under the same conditions with set-point = 0.9.

were performed at set-point of 0.9 and the measurements of phase contrast were performed at a set-point of 0.6.

Next, we prepared a silicon surface with adjacent PS and PB films of about 400 nm thickness such that we could image all three materials in the same experiment. Fig. 12 shows images of this sample where we can clearly differentiate the three materials in the phase image. Fig. 13 shows the section of phase image along the dotted line in Fig. 12(b). The phase contrast between the PB and the silicon is 19° and that between the PS and the silicon is 5°. These results compare well with the simulations as shown previously in Fig. 4.

The next polymer that we studied was the butadiene–styrene–butadiene block copolymer. Cast films of this material are in the disordered state with no microphase separation. Upon annealing though, distinct domains of the polybutadiene blocks and the polystyrene blocks form due to the immiscibility of polybutadiene and polystyrene under the annealing conditions. We imaged the cast film before and after annealing, producing the images in Fig. 14. The microphase domains are clear in the phase image of the annealed films. Even a portion of the film (on the right) that is so thin that it is barely visible in height is clearly visible in the phase image. The sections of the phase images in Fig. 14 are shown in Fig. 15. The film in the disordered state has a phase contrast relative to silicon of 16.5° which is between the values for pure PS(5°) and pure PB(19°), In Fig. 15(b), we can clearly see the distinction between the micro-domains consisting of PB and those of PS each of which have approximately the same values as do the pure polymers.

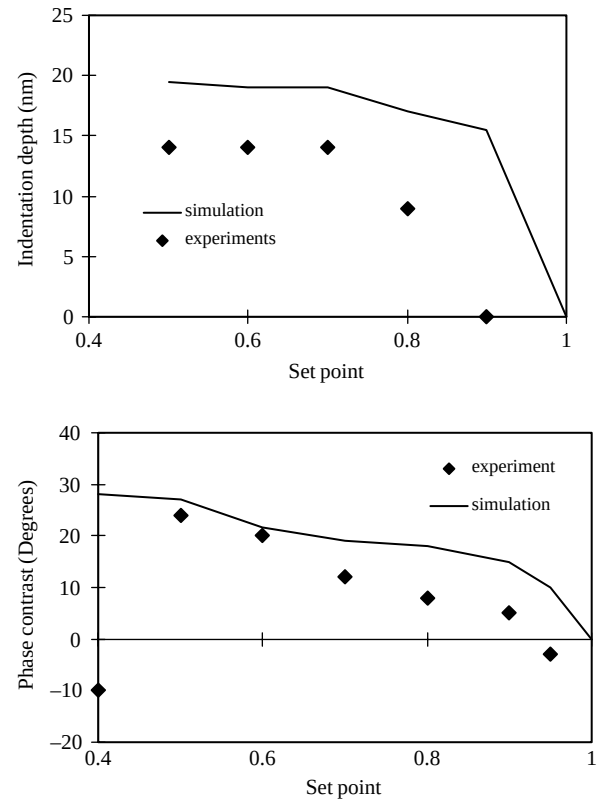

Fig. 8. Phase contrast and indentation depth as a function of set-point for polystyrene on silicon.

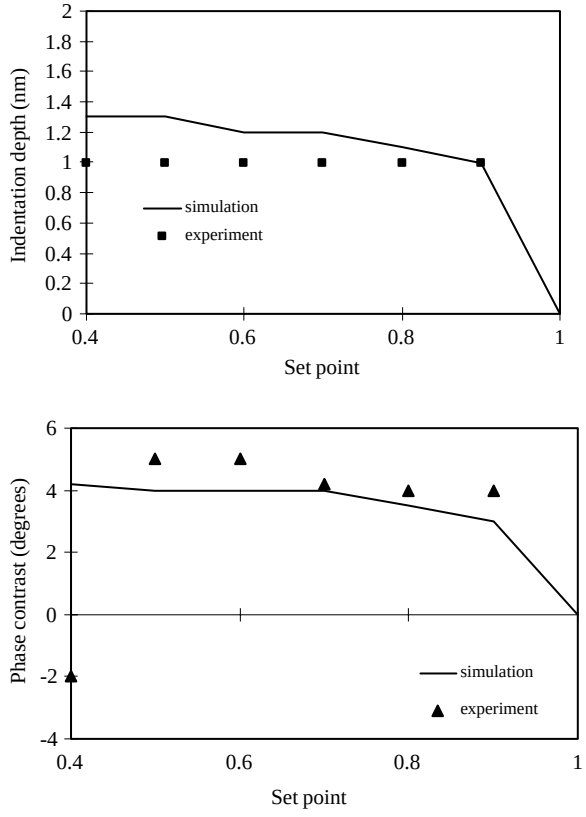

Fig. 9. Phase contrast and indentation depth as a function of set-point for polystyrene on silicon.

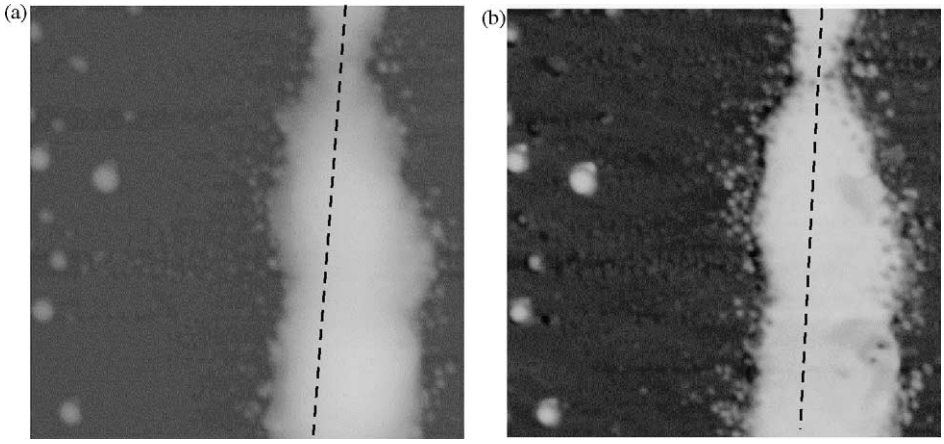

Fig. 10. Topography (a) and phase (b) images of polybutadiene (bright) on silicon, free vibration amplitude 90 nm, set-point 0.9 for topography image and 0.6 for phase image. Grayscale is 0–300 nm for topography image and 0–50° for phase image. Dashed lines indicate sections taken for Fig. 11.

This is expected even though the blocks of PB and PS have different molecular weights than the respective pure polymers since the properties that we are probing here are the high frequency properties, which are dependent on the monomer chemistry rather than the larger scale structure. Additionally, in the region where the film is very thin we see smaller phase contrast for both PS and PB domains. This is the same phenomena we observed earlier with the PB film of varying thickness.

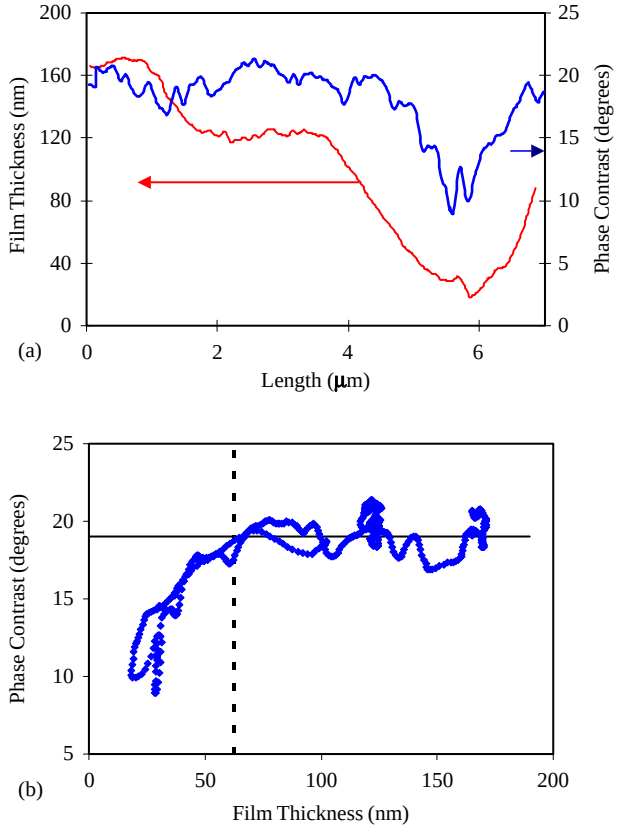

Fig. 11. Effect of polybutadiene film thickness on the phase contrast. (a) Section analyses of the images in Fig. 10 along the dotted lines from the bottom of the images up. (b) Data from (a) replotted in terms of phase contrast vs film thickness. Solid horizontal line in (b) indicates the thickness independent value of the phase contrast (19°). Dotted line in (b) indicates the approximate thickness of a layer of three molecules.

6. Inferring material properties from phase contrast

The ultimate goal of this work was to develop a procedure for inferring the local viscoelastic properties from the TM-AFM phase image. As explained earlier the experimental procedure requires (1) using a stiff, known material as an internal standard reference for phase contrast and (2) selecting the operating conditions such that the tip–sample interaction force is dominated by the mechanical properties. Also, we have constructed and validated a model for the vibration of the cantilever and the resulting phase contrast with silicon given a polymer of known viscoelastic properties. The next step is to apply the model to unknown materials and infer their local properties. One way to do this is to perform the direct numerical simulation of the vibration within an optimization routine to fit experimental results. As an alternate approach, we have created a correlation for phase contrast with respect to silicon as a function of storage modulus by performing simulations for a wide range of possible viscoelastic properties.

The first step in the development of the correlation is to simplify the model because as it stands we have too many unknown parameters: $G'(1/t_c)$, $G''(1/t_c)$ and ν. The most appropriate way to do this is to assume that $G''(1/t_c) \ll G'(1/t_c)$ This assumption is valid for most materials at these

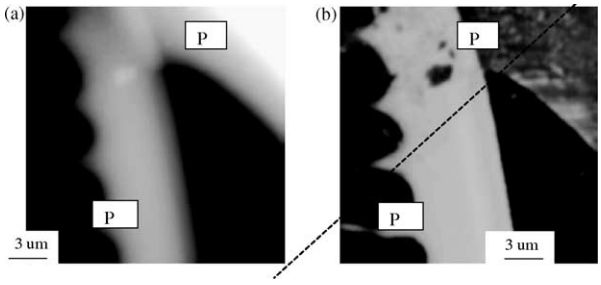

Fig. 12. Topography (a) and phase (b) images of PS and PB on silicon at set-point 0.6. Grayscale is 0–700 nm for topography image and 0–40° for phase image.

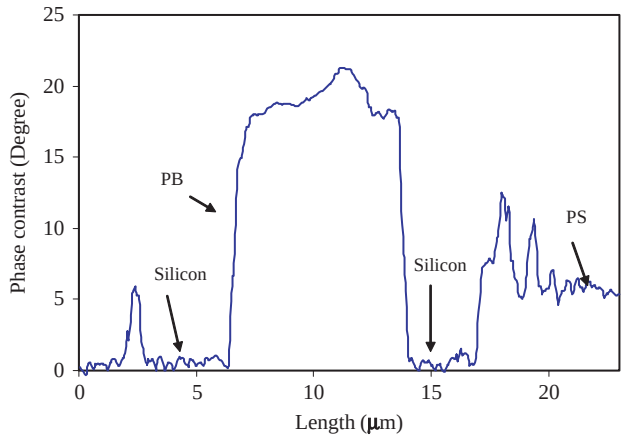

Fig. 13. Section analysis of the phase image in Fig. 12 along the dotted line from bottom of the image to the top.

high frequencies where polymers usually exhibit either rubbery plateau behavior (as PB) or glassy behavior (as PS). Now we are left with the following relation for the viscosity

$$\eta = G' t_c \tag{9}$$

and the Young's modulus is still given by Eq. (7). For the Poisson's ratio, a value of 0.5 is valid for rubbery polymers and a value of approximately 0.3 is valid for many glassy polymers. We have performed simulations for both values, and then developed the correlation in terms of the reduces storage modulus ($G'/(1-\nu)$). We have assumed values for the van der Waals parameters: $a_0 = 0.234 \times 10^{-9}$ m and $H = 6.16 \times 10^{-20}$ J which are appropriate for polymers [8,14]. The results are shown in Figs. 16 and 17. Correlation between reduced storage modulus and phase contrast (ϕ) is:

$$\log\left[\frac{G'}{1-\nu}\right] = 0.00581\phi^2 - 0.308\phi + \frac{1.03}{\phi} + 10.238 \tag{10}$$

The correlation for the contact time in terms of the phase contrast is:

$$t_c = \frac{1}{\omega_0}(-0.00145\phi^2 + 0.105\phi + 0.2325) \tag{11}$$

In the preceding two equations the units of phase contrast are degrees, the units of modulus are Pa, the units of time are seconds and the units of frequency are rad/s. By using these two correlations one can estimate the local properties of unknown materials from their phase contrast relative to silicon. We note that this technique, however, does not provide a route for estimating the Poisson's ratio. Therefore, in order to find the modulus rather than the reduced modulus one must have another source for information about this property.

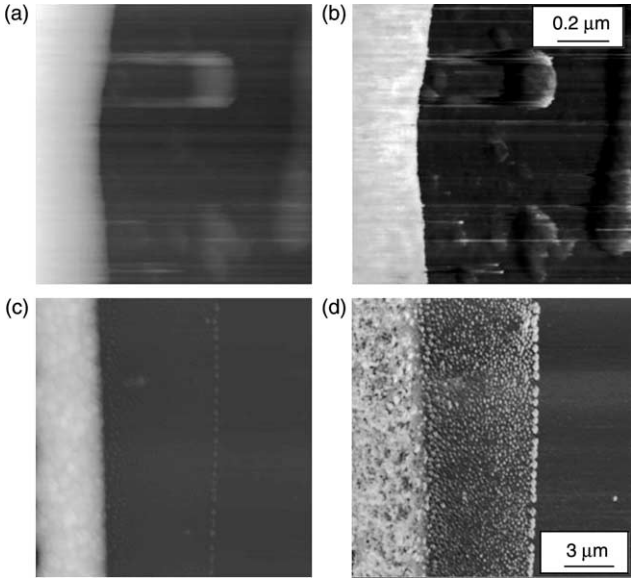

Fig. 14. Topography (a and c) and phase image (b and d) of PB–PS–PB block copolymer on a silicon surface. (a) (b) before annealing and (c) (d) after annealing. Grayscale is 0–300 nm for topography image and 0–40° for phase image. Note the difference in scale.

7. Application to experimental materials

Now, we apply the correlations developed in the last section to our experimental data. The results for the films that were thick enough such that the phase contrast was independent of thickness are presented in Table 3. For the PB the differences between our inferred modulus and viscosity and those measured in small amplitude oscillatory shear are 5 and 15%, respectively. For PS the difference in these measurements are 7% for both modulus and viscosity. This indicates that our procedure can be expected to work well for materials with a shear modulus between 1 and 1000 MPa. Outside of this range the performance becomes less reliable.

Next, we consider the results of the block copolymer for which we do not have small amplitude oscillatory shear data. Instead we compare the behavior of the block copolymer in a disordered state to that of the individual microdomains in the phase separated state. To do this comparison we use the following mixing rule for viscosity, which is known to be valid for entangled polymers

$$\eta_B^{1/\alpha} = w_1 \eta_1^{1/\alpha} + w_2 \eta_2^{1/\alpha} \tag{12}$$

where w refers to weight fraction, the index B refers to blend and $\alpha = 3.4$. The disordered block copolymer can be considered to be a blend of PS and PB with the weight fractions given by the lengths of the blocks ($w_{PS} = 0.136$, $w_{PB} = 0.864$). The viscosities of the PS and PB components can then be estimated from $\eta = G' t_c$ where the G' is that measured for the relevant micro-domain in the phase separated state and t_c is the contact time in the disordered state. In this way, we find $\eta_{PB} = 1.45$ Pa s and PS = 622 Pa s at a contact time of 7.41×10^{-7} s. (Note that the viscosity values presented in Table 3 for the micro-domains are at 7.91×10^{-7} s and 3.34×10^{-7} s for the polybutadiene and polystyrene domains, respectively). Then from Eq. (12), we estimate that the viscosity of the block copolymer in the disordered state should be 2.26 Pa s. This compares very well with 2.34 Pa s, which is inferred from the phase contrast of the

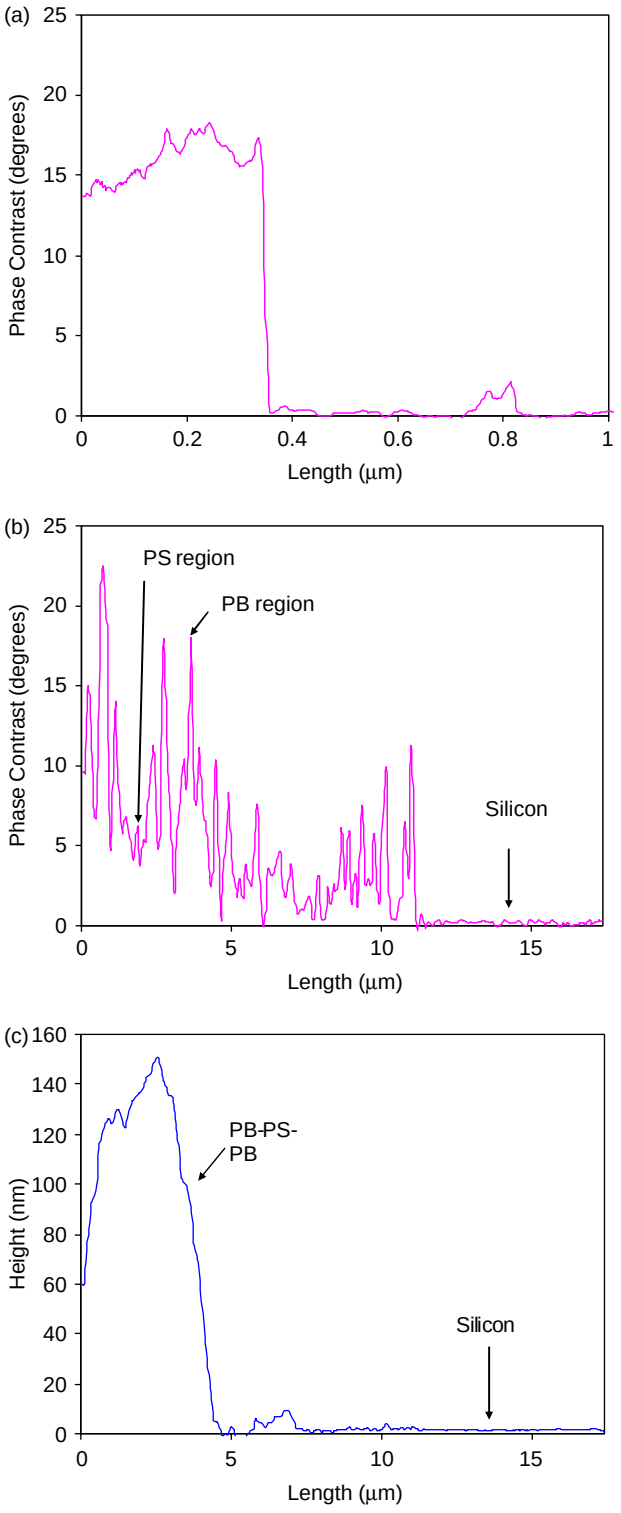

Fig. 15. Section analysis for PB–PS–PB block copolymer on silicon surface. (a) Phase section before annealing, (b) phase section after annealing, (c) height section after annealing.

disordered block copolymer. This result adds further evidence to our conclusion that the technique is performing very well and also demonstrates its potential for use with complex materials where larger scale measurements of viscoelastic properties may not be possible.

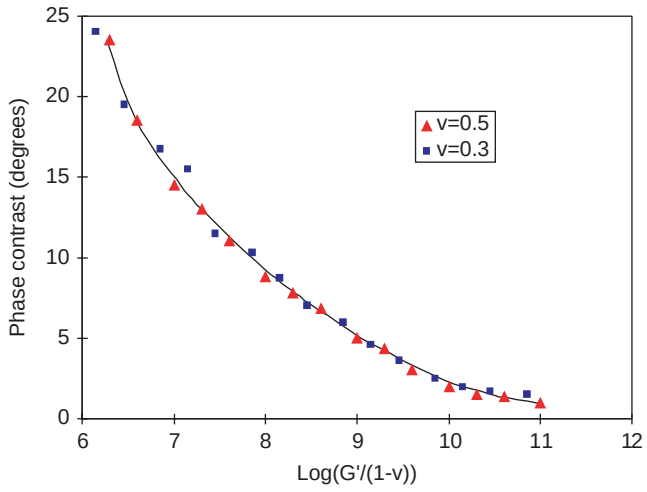

Fig. 16. Relationship between phase contrast relative to silicon and the logarithm of reduced storage modulus (Pa). Points are results of simulations for two different Poisson's ratios. Curve represents Eq. (10).

Now, we move on to the results shown in Fig. 11 for the relation between film thickness and phase contrast for PB. From these data we infer the viscoelastic properties shown in Fig. 18. In order to interpret these results we must consider the well known apparent stiffening that is observed when measuring the modulus of a thin, soft sample on a hard substrate. The Hertzian model that we use to describe the elastic force assumes an infinitely thick sample. The strain and stress fields during indentation of a soft sample of finite thickness can be significantly different from the Hertzian case, rendering the elastic portion of the DMT model invalid. For such cases, if the elastic modulus is calculated from indentation data using the Hertzian approach the modulus will be artificially high. Dimitriadis et al. [15] analyzed this phenomenon for soft samples and developed the following correction formula using the integral transform method to

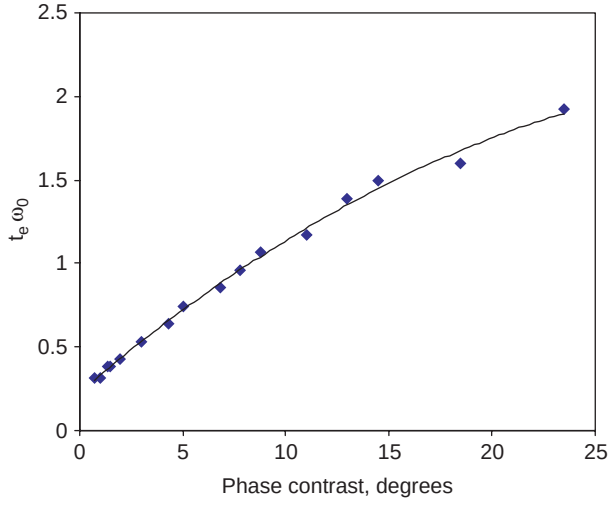

Fig. 17. Relationship between contact time and phase contrast. Symbols are results from simulations and line represents Eq. (11).

Table 3
Inferred local properties

Sample		ϕ	$G'/1-v$ (MPa)	V	G' (MPa)	η^* (Pa s)
Polybutadiene		20	3.12	0.5	1.560	1.28
Polystyrene		4.5	1580	0.3	1106	350
Disordered block copolymer		16.5	6.31	0.5	3.16	2.34
Micro-phase separated block copolymer	PB domains	18.4	3.9	0.5	1.96	1.55
	PS domains	4.9	1198	0.3	839	280

Values for Poisson's ratio (v) are assumed here.

develop an analytical solution of the elastic problem.

$$\frac{E_{app}}{E} = 1 + 1.113\chi + 1.283\chi^2 + 0.769\chi^3 + 0.0975\chi^4 \qquad (13)$$

where

$$\chi = \frac{\sqrt{R\delta}}{h}$$

In this equation, E_{app} is the measured modulus, E is the true modulus, R is the radius of the tip, δ is the indentation depth and h is the thickness of the sample. The coefficients were determined for the case of a bonded sample (i.e. one that will not slide) of $v=0.5$. We use this equation to estimate the effect of this phenomenon on our experiments on PB by assuming that $R=10$ nm, according to manufacturers specifications, and $\delta=14$ nm, according to our experimental results (Fig. 8). On Fig. 18, the solid line shows the modulus that we would expect to measure for our film if the stiffening effect due to the substrate were the only factor causing the higher than bulk modulus. It is clear that the substrate effect accounts for only a small portion of the stiffening effect and that the actual modulus of the thin film is different from that in bulk. This is not surprising as polymer chains near to solid walls are known to exhibit constrained conformations [16], which could result in a local stiffening in the normal direction.

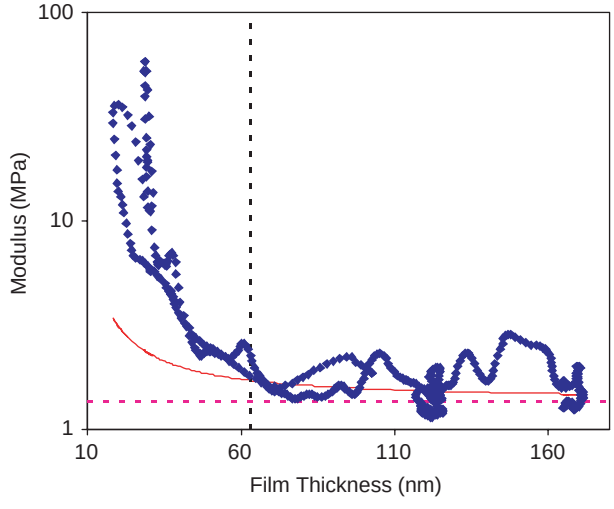

Fig. 18. Relationship between apparent modulus and film thickness for polybutadiene. Symbols are experimental results from Fig. 11(b) after applying Eq. (10) and assuming $v=0.5$. Vertical dotted line represents the approximate thickness of a layer of three unperturbed molecules and horizontal dotted line indicates bulk value of modulus. The solid line shows the apparent modulus predicted from Eq. (13).

It is also possible to use Eq. (13) to correct our measured data for the substrate effect, leaving only the effect of constrainment of the chains. The corrected modulus values are shown in Fig. 19(a). The viscosity was calculated from the corrected moduli using Eqs. (9) and (11) and the results are shown in Fig. 19(b). Note that in this analysis we have assumed that the relationship between contact time and phase lag is unaffected by the thickness of the film. This is reasonable because it is the contact stiffness that determines this relationship independent of the fundamental nature of the contact. These data also demonstrate the power of this technique in studying phenomena that cannot be studied at larger scales.

In order to further investigate this phenomenon, we consider a set of data from Satomi et al. [17] who studied the effect of substrate modulus on the surface modulus of a polystyrene film on a silicon substrate measured with an alternate AFM based technique [18]. The data from Fig. 6 of Satomi et al. [17] have been extracted and plotted in our Fig. 20 where they are compared to the substrate stiffening effect predicted with Eq. (13) modified for a Poisson ratio of 0.3 [15]. Their data have also been corrected for the substrate effect and plotted in the same figure. We can note several interesting aspects of this result. First, we see a significant stiffening of the film likely due to the molecular constraint for films between 45 and 80 nm thick. (Note that the radius of gyration of this polystyrene is approximately 11 nm, which is very close to that of our polybutadiene at 10.5 nm). While this stiffening is significant, about 3.5 times at its maximum, it is not as severe as that observed in the case of polybutadiene which was up to 35 times. Also, the stiffening of polystyrene appears to start at thicker films ($8R_g$) than it does in the case of polybutadiene ($6R_g$). Finally, the polystyrene exhibits an interesting softening behavior in films thinner than 45 nm, which has been attributed to a lowering of the glass transition temperature. We note at this point, that Satomi et al. [17] attributed all of the observed stiffening to the substrate effect. It is clear though from the work of Dimitriadis et al. [15] and Wang et al. [19] that the magnitude of the substrate stiffening effect is related to the ratio of the contact diameter to the film thickness and that it only becomes significant at a ratio of about 0.1. Considering the reported tip radius (18 nm) and indentation depth (1 nm) [17] it is expected that the substrate effect is small here.

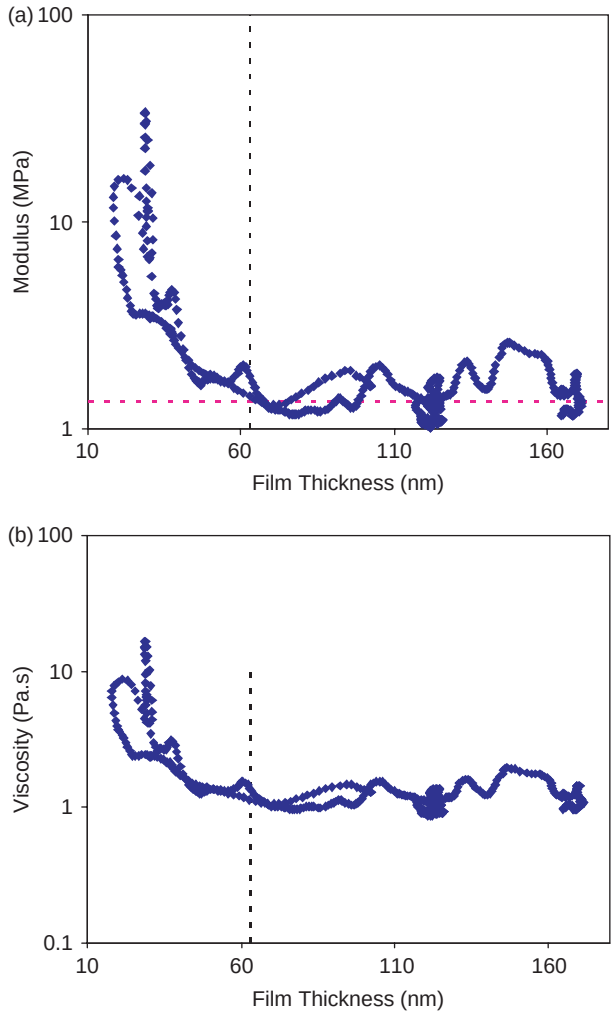

Fig. 19. (a) Relationship between modulus and film thickness for polybutadiene. Symbols are experimental results from Fig. 11(b) after applying Eq. (10), correcting with Eq. (13) and assuming $\nu = 0.5$. Vertical dotted line represents the approximate thickness of a layer of three unperturbed molecules and horizontal dotted line indicates bulk value of modulus. (b) Relationship between viscosity and film thickness for polybutadiene. Symbols are experimental results calculated using Eq. (9), the corrected moduli from part (a) and the contact time as in Eq. (11).

8. Influence of probe parameters on the correlations

The correlations presented in the last section are only useful if they are not dependent on certain aspects of the operating conditions. In particular, we wish to demonstrate that they are not dependent on the cantilever over a reasonable range of its parameters. It is first important to define the fundamental parameters; these are the friction coefficient, c, the effective

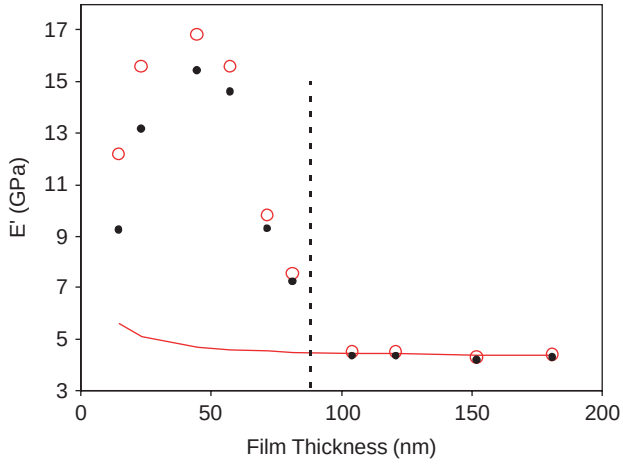

Fig. 20. Analysis of data from Fig. 6 of Satomi et al. [17]. Open symbols are their original data. Solid symbols are their data corrected for substrate stiffening effect. Solid curve shows the apparent modulus predicted by Eq. (13) modified for a Poisson ratio of 0.3 [15] assuming a tip radius of 18 nm and an indentation depth of 1 nm. Dashed vertical line shows the thickness of a layer of four unperturbed molecules.

mass, m, and the cantilever stiffness, k. These parameters are related to the parameters in Eq. (1) as shown below:

$$Q = \frac{\sqrt{mk}}{c} \tag{14}$$

$$\omega_0 = \sqrt{\frac{k}{m}\left(1 - \frac{1}{2Q^2}\right)} \tag{15}$$

The friction coefficient depends on the geometry of the cantilever and the viscosity and density of the medium in which the cantilever is immersed (here it is air but it could feasibly be other fluids). The effective mass is of course dependant on the geometry and density of the cantilever and the stiffness, k, depends on the Young's modulus of the cantilever and its geometry. It is not practical physically to change these three parameters independently so here we consider the case of (1) a heavier and stiffer cantilever and (2) a lighter and less stiff cantilever. The parameter set in Table 2 corresponds to $c = 4.68 \times 10^{-5}$ g/s and $m = 8.76 \times 10^{-9}$ g which comprises our base values along with $k = 40$ N/M for our parametric study. For case 1 (heavier, stiffer cantilever) we simply multiplied the mass and the stiffness of our base cantilever by 1.5 and for case 2 (lighter, less stiff) we divided those two parameters by 1.5. We then simulated the forced vibration of the cantilevers in case 1 and case 2 in contact with surfaces of varying stiffness. The results shown in Table 4 demonstrate clearly that our

Table 4
Parametric study of effect of cantilever characteristics on the phase contrast curve

Case	m (ng)	k (N/m)	Q	ω_0 (kHz)	ϕ (°)		
					$G/1-\nu = 2$ GPa	$G/1-\nu = 60$ MPa	$G/1-\nu = 2$ MPa
Base	8.76	40	400	340	3.5	11	23.5
1	13.15	60	600	340	4	12	24
2	5.84	26.7	266.7	340	4	12	24

technique for inferring local properties is insensitive to small changes in the cantilever properties.

9. Conclusions

A technique has been developed and validated for inferring local mechanical properties from tapping mode atomic force microscope images of viscoelastic surfaces. This technique is based upon a theoretical model of the forced oscillation of the micro-cantilever and its contact with the surface. It is shown that by operating under low set-point conditions where the mechanical response of the surface dominates the tip-surface interaction and by using a stiff internal reference surface one can determine unambiguously and with reasonable accuracy the high frequency local viscoelastic properties of the surface. The technique was used to infer the properties of micro-phase separated domains in a poly(butadiene–styrene–butadiene) block copolymer. The influence of sample thickness was estimated and an approach for correcting for the apparent stiffening due to non-Hertzian strain and stress fields was presented. Using this correction, the effect of molecular constraint on the modulus of an ultra-thin polybutadiene film is measured.

Acknowledgements

The authors gratefully acknowledge funding provided by The Taiho Kogyo Tribology Research Foundation and by NSERC.

References

[1] Garcia R, Parez R. Dynamic atomic force microscopy methods. Surf Sci Rep 2002;197–301.
[2] Sheiko SS. Imaging of polymers using scanning force microscopy: from superstructures to individual molecules. Advances in polymer science. Berlin, Heidelberg: Springer-Verlag; 2000 p. 62–159.
[3] Bar G, Brandsh R, Whangbo M-W. Effect of viscoelastic properties of polymers on the phase shift in tapping mode atomic force microscopy. Langmuir 1998;7343–7.
[4] Berquanda A, Mazerana P-E, Laval J-M. Influence of volume and surface properties on phase contrast. Surf Sci 2003;523:125–30.
[5] Wanga L. Analytical descriptions of the tapping-mode atomic force microscopy response. Appl Phys Lett 1998;73(25).
[6] Benmouna F, Johannsmann D. Dynamic atomic force microscopy methods. Langmuir 2004;20:188–93.
[7] Tamayo J, Garcia R. Deformation contrast, and phase contrast in tapping mode scanning force microscopy. Langmuir 1996;12:4430–5.
[8] Scott WW, Bhushan B. Use of phase imaging in atomic force microscopy for measurement of viscoelastic contrast in polymer nanocomposites and molecularly thick lubricant films. Els Sci 2003;151–69.
[9] Raghavan D, Vanlandingham M, Gu X, Nguyen T. Characterization of heterogeneous regions in polymer systems using tapping mode and force mode atomic force microscopy. Langmuir 2000;16:9448–59.
[10] Dubourg F, Aime JP, Marsaudon S, Boisgard R, Leclere P. Probing viscosity of a polymer melt at the nanometer scale with an oscillating nanotip. Eur Phys J 2001;E6:49–55.
[11] Dubourg F, kopp-Marsaudon S, Leclere Ph, Lazzaroni R, Aime P. Experimental determination of the viscosity at the nanometer scale on a block copolymer with an oscillating nanotip. Eur Phys J 2001;E6:387–97.
[12] Garcia R, San Paulo A. Attractive and repulsive tip–sample interaction regimes in tapping-mode atomic force microscopy. Phys Rev B 1991;4961–7.
[13] Stark RW, Schitter G, Stemmer A. Tuning the interaction forces in tapping mode atomic force microscopy. Phys Rev, B 2003;68.
[14] San Paulo A, Garcia R. Tip-surface forces, amplitude, and energy dissipation in amplitude-modulation force microscopy. Phys Rev B 2001; 64:193411–21.
[15] Dimitriadis EK, Horkay F, Maresca J, Kacher B, Chadwick RS. Determination of elastic moduli of thin samples using the atomic force microscope. Biophys J 2002;2798–810.
[16] Granick S, Kumar SK, Amis EJ, Antonietti M, Balazs AC, Chakraborty AK, et al. J Polym Sci, Part B: Polym Phys 2003;41: 2755–93.
[17] Satomi N, Tanaka K, Takahara A, Kajiyama T. Effect of internal bulk phase on surface viscoelastic properties by scanning probe microscopy. Macromolecules 2001;34:6420–3.
[18] Kajiyama T, Tanaka K, Takahara A. Surface molecular motion of the monodisperse polystyrene films. Macromolecules 1997;30:280–5.
[19] Wang M, Liechti KM, White JM, Winter R. Nanoindentation of polymeric thin films with an interfacial force microscope. J Mech Phys Sol 2004;52:2329–54.